



HAL
open science

EXPERIMENTAL CHARACTERIZATION AND ANALYTICAL MODELING OF ROTOR TONAL NOISE

Benjamin Cotté, Tommy Rigall, Chakshu Deora

► **To cite this version:**

Benjamin Cotté, Tommy Rigall, Chakshu Deora. EXPERIMENTAL CHARACTERIZATION AND ANALYTICAL MODELING OF ROTOR TONAL NOISE. Forum Acusticum 2020, Dec 2020, Lyon, France. pp.2615-2621. hal-03336256

HAL Id: hal-03336256

<https://hal.science/hal-03336256>

Submitted on 10 Sep 2021

HAL is a multi-disciplinary open access archive for the deposit and dissemination of scientific research documents, whether they are published or not. The documents may come from teaching and research institutions in France or abroad, or from public or private research centers.

L'archive ouverte pluridisciplinaire **HAL**, est destinée au dépôt et à la diffusion de documents scientifiques de niveau recherche, publiés ou non, émanant des établissements d'enseignement et de recherche français ou étrangers, des laboratoires publics ou privés.

EXPERIMENTAL CHARACTERIZATION AND ANALYTICAL MODELING OF ROTOR TONAL NOISE

Benjamin Cotté¹

Tommy Rigall¹

Chakshu Deora¹

¹ IMSIA, ENSTA Paris, CNRS, CEA, EDF, Institut Polytechnique de Paris, France

benjamin.cotte@ensta-paris.fr

ABSTRACT

In this study, the tonal noise due to the interaction of a simplified rotor and a circular tower is characterized experimentally in a controlled environment. The test bench is installed in the anechoic chamber of ENSTA Paris, and is composed of a rotor made of three NACA 0012 untwisted blades set into motion by a motor. The radiated noise is measured by three microphones and 32 pressure taps are mounted on the tower wall to measure the pressure variation during the blade passage. The effect of the blade-tower distance is clearly captured in the wall and acoustic pressure measurements, blade-tower interaction noise being significant when the distance is smaller than the tower radius. Based on the measured wall pressure distribution on the tower surface, the acoustic pressure is calculated using Curle's analogy in the compact far-field approximation. The contribution of the blades in the noise generation is not considered. The measured and predicted spectra are in good agreement, although the magnitude of the Fourier series coefficients of harmonics 3 to 6 tends to be overpredicted.

1. INTRODUCTION

In open rotor applications such as axial fans, marine propellers or wind turbines, the main noise mechanisms can be separated into tonal and broadband components. Tonal noise is characterized by discrete frequency peaks at the blade passage frequency (BPF) and its harmonics, and is generally dominated at low Mach number by unsteady loading noise mechanisms that can be due to rotor-structure interactions, such as blade-tower interaction noise in the case of wind turbines [1–3], or the interaction of the rotors with their supporting struts for drone noise [4].

The blade-tower interaction noise can be decomposed into two aerodynamic phenomena that cause unsteady loading on the blades and on the tower [2, 3]. The first one is the blade-passage effect that is related to the aerodynamic disturbance generated by the blades passing in the vicinity of the tower. The second one is the reduced velocity field upwind of the tower that causes a sudden change in the angle of attack of the passing blade. In this study, we focus on the tonal noise associated with the blade-passage effect, that is characterized experimentally in a controlled environment using a simplified rotor with a small blade pitch set into motion by a motor.

The objective of this work is to study the influence of the blade-tower distance on the radiated noise and on the distribution of the wall pressure on the tower surface. For this purpose, 32 pressure taps are mounted on the tower wall to measure the wall pressure fluctuations during the blade passage, and the acoustic pressure is measured using three microphones. Based on the wall pressure distribution on the tower surface, the contribution of the tower to the overall acoustic pressure is calculated using Curle's analogy.

The structure of the paper is as follows. First, the experimental setup is presented in Section 2, and the data analysis is described in Section 3. Then, the semi-analytical model for blade-tower interaction noise is presented in Section 4, and the comparison between model predictions and measurements is shown in Figure 5.

2. EXPERIMENTAL SETUP

The experimental setup consists in a three-bladed open rotor operated by a 3 kW motor, as shown in Figure 1. The setup is installed in the anechoic chamber of IMSIA at ENSTA Paris, whose dimensions are 3.5 m × 3.0 m × 2.6 m. This anechoic chamber provides a near reflection-free environment up to a minimum frequency of approximately 100 Hz.

The rotor blades used in these experiments are three untwisted NACA 0012 airfoils of chord 0.07 m and span 0.4 m. The blades are mounted using a rig of radius 0.035 m manufactured for a pitch angle of 3°. In this study, the rotation speed is chosen as 900 rotations per minute (RPM), which corresponds to a tip Mach Number of 0.12 and a chord-based tip Reynolds number of 1.9×10^5 . Since the Reynolds number is relatively low, the blades are tripped at 10% of the chord on both sides of the blades to avoid laminar boundary layer instabilities.

In order to study the blade-tower interaction mechanisms, a tower of diameter $D = 11$ cm is mounted on a translating cart so as to adjust the blade-tower distance. Blade-tower distance d is measured from the trailing edge of the blade to the tower, as shown in Figure 2. In this set of experiments, the blade-tower distance d is varied between $2D/7$ and D as in Yauwenas *et al.* [2] and Zajamsek *et al.* [3].

In order to characterize the aerodynamic disturbance due to the blade passing in front of the tower, 32 pres-

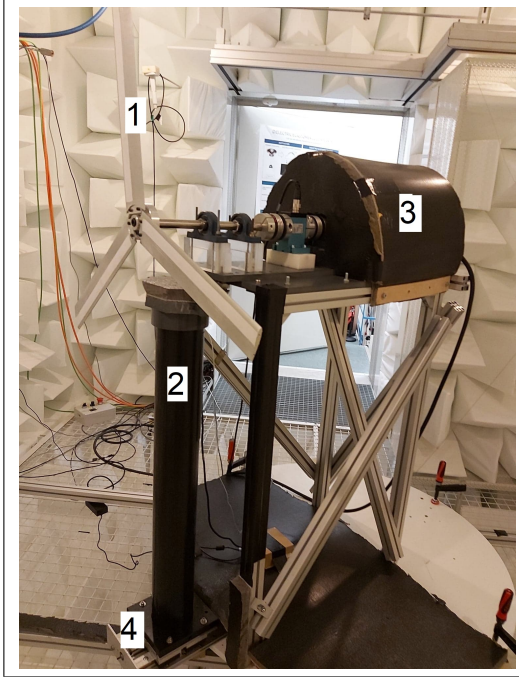


Figure 1. View of the experimental setup: 1. NACA 0012 blades, 2. tower, 3. 3kW motor covered by absorbing material, 4. translating cart for the tower.

sure taps are mounted on the tower, whose spatial distribution is shown in Figure 3. The curvilinear abscissa along the tower surface is noted s , and $z = 0$ is taken on the rotor axis. The taps are located between $s = -6.6$ cm and $s = +6.6$ cm, which corresponds to angles θ between -69° and 69° , thus covering a large portion of the tower surface. When the blade is pointing downwards, the tip of the blade is at $z = -43.5$ cm, between pressure taps 1 and 2. The pressure variations are acquired using a ZOC22b Scanivalve pressure scanner at a sampling frequency of 2 kHz.

The acoustic pressure is measured using three Brüel & Kjær free-field 1/2" microphones at a sampling frequency of 48 kHz. The microphone positions are given in Table 1. The first one is placed in the rotor plane, the second one is on the rotor axis and the third one is 44 cm in front of the rotor, and 1.1 m below the rotor axis.

Microphone	Cartesian coordinates (x, y, z)
1	$(0, 1.2 \text{ m}, 0)$
2	$(1.2 \text{ m}, 0, 0)$
3	$(0.44 \text{ m}, 0, -1.1 \text{ m})$

Table 1. Microphone positions used in the experiment. The coordinate system (x, y, z) is shown in Figure 2, and the origin is taken at the rotor center.

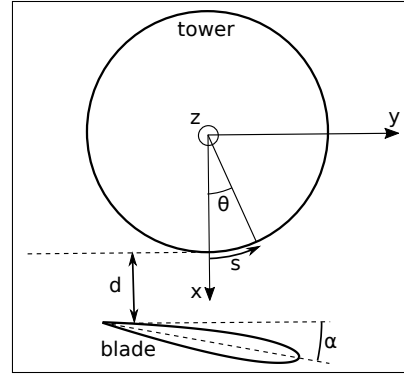


Figure 2. Schematic for blade-tower distance d , top view. The blade is moving from the left to the right (rotation in the counter-clockwise direction) and its pitch angle is noted α .

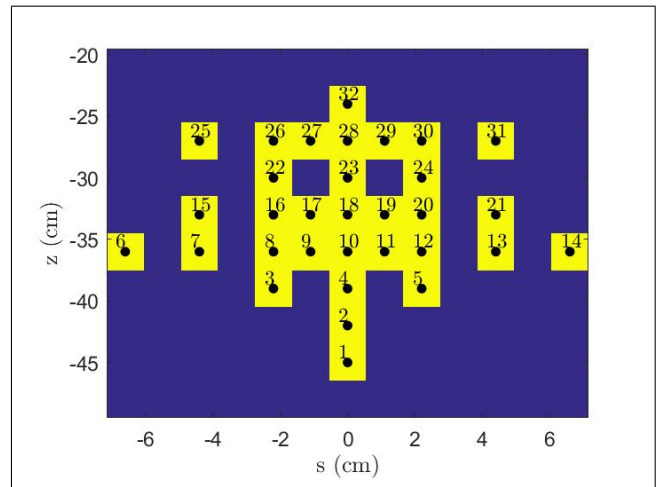


Figure 3. Positions of the 32 pressure taps along the tower surface (unwrapped front view).

3. DATA ANALYSIS AND SIGNAL PROCESSING

3.1 Wall pressure signals

First, it is interesting to look at the spectrum levels of the wall pressure for various blade-tower distances d , as shown in Figure 4. As expected, tones are found at the harmonics of the blade-passing frequency $\text{BPF} \approx 45.35$ Hz, and the tonal peak amplitudes are reduced when d increases. It appears that the measurements are very noisy, with a noise floor around 100 dB. The signal-to-noise ratio is degraded when d increases, so that the measurements at $d = D$ can hardly be exploited.

In order to improve the signal-to-noise ratio, time-synchronous averaging (TSA) is performed based on the duration $T_{\text{BPF}} = 1/\text{BPF} \approx 22.1$ ms between the passing of two successive blades. The signals contain approximately 1800 periods of duration T_{BPF} , but it is not possible to perform TSA over the entire signal because there is a small time shift between successive periods. As a result, TSA is performed on only 100 successive periods of duration T_{BPF} , which yields a total of 18 averaged signals. A small time shift of approximately 5 ms is noticed be-

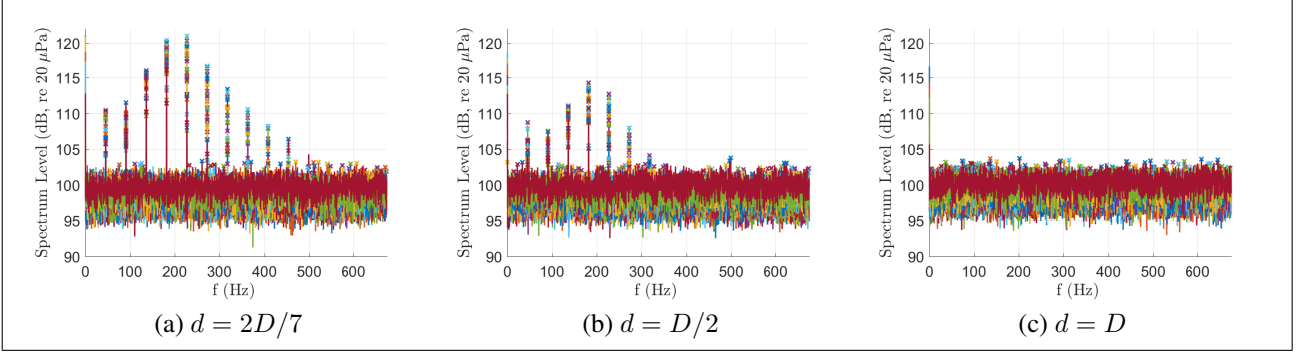


Figure 4. Spectrum level for the 32 wall pressure taps at various blade-tower distances d .

tween each signal, that can be attributed to the uncertainty on the value of T_{BPF} . Once this time shift is corrected, the 18 signals overlap quite well, as can be seen in Figure 5(a) for taps 7, 10 and 13, and it is possible to calculate the mean wall pressure over these 18 signals. A clear time shift between tap 7 at $s = -4.4$ cm, tap 10 at $s = 0$ and tap 13 at $s = +4.4$ cm is observed in Figure 5(a), that is consistent with the counter-clockwise direction of rotation of the blades. Also, the wall pressure amplitude is greater at tap 10 located at $s = 0$.

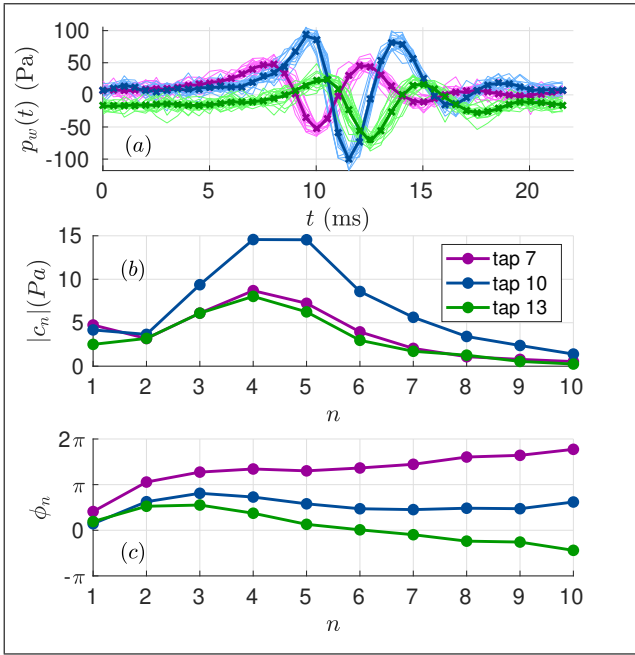


Figure 5. (a) Wall pressure waveforms obtained by TSA (thin solid lines), mean over the 18 signals (thick solid lines), and Fourier synthesis over harmonics 1 to 10 (crosses), (b) magnitude and (c) phase of the Fourier series coefficients $c_n = |c_n|e^{i\phi_n}$ for $d = 2D/7$.

As the signals are periodic, it is possible to calculate the complex Fourier series coefficients $c_n = |c_n|e^{i\phi_n}$ of the wall pressure. The magnitude and phase of these coefficients are plotted in Figures 5(b) and (c) respectively for taps 7, 10 and 13. The harmonics 3 to 6 are seen to dominate, and the magnitudes of the coefficients for tap 10 is approximately twice the ones for tap 7 and 13. A shift

is also visible between the phases of taps 7, 10 and 13 in Figure 5(c), that reflects the time difference seen in Figure 5(a). Finally, when the wall pressure signals are synthesized using the 10 first components of the Fourier series, a very good agreement is obtained compared to the original signal, as can be seen in Figure 5(a).

The maps of the magnitude $|c_n|$ and phase ϕ_n of the Fourier series coefficients of the harmonics 4 and 5 are plotted in Figure 6 for the blade-tower distance $d = 2D/7$. The values obtained from the measurements at the 32 pressure taps are numbered from 1 to 32, while the other values are obtained using an extrapolation procedure explained below. Figures 6(a) and (b) show that the magnitude $|c_n|$ is maximum close to the center $s = 0$, and reaches a maximum at the height of tap 10, corresponding to approximately 80% of the blade length. Let us introduce the function $F_n(s, z) = |c_n(s, z)|/|c_n(0, z)|$ that characterizes the distribution of $|c_n|$ along s at a given height z . This function can be averaged over the heights where measurements are available to obtain $\langle F_n \rangle(s)$, the mean distribution of $|c_n|$ along s . This mean distribution is plotted in Figure 7 for n between 3 and 6. Note that values at $s = \pm 6.6$ cm are obtained from only one measurement, and that values at $s = \pm 5.5$ cm and $s = \pm 3.3$ cm where no measurement is available are obtained from linear interpolation. It can be observed that the decay of $|c_n|$ with respect to s is not symmetrical, with a faster decay towards negative values. Also the magnitude of the Fourier series coefficients c_n tends to decrease faster as n increases. Using the mean relative magnitude $\langle F_n \rangle(s)$ and the measured value of $|c_n|$ at $s = 0$, the complete map of $|c_n|$ over the tower surface is deduced, as shown in Figure 6(a) and (b) for $|c_4|$ and $|c_5|$ respectively.

Focusing now on the phase maps for the harmonics 4 and 5 in Figure 6(c) and (d), we observe a gradual decrease when the blade moves from negative to positive values of s , as already seen in Figure 5(c) between taps 7 and 13. It is thus meaningful to calculate the mean value of the phase $\langle \phi_n \rangle$ at a given position s from the available measurements at various heights. The mean value of the phase $\langle \phi_n \rangle(s) - \langle \phi_n \rangle(0)$ is plotted with respect to s in Figure 7 for harmonics 3 to 6. The phase difference is seen to increase when n increases. Also, there is a change of slope at the extreme values $s = \pm 6.6$ cm. However, since there

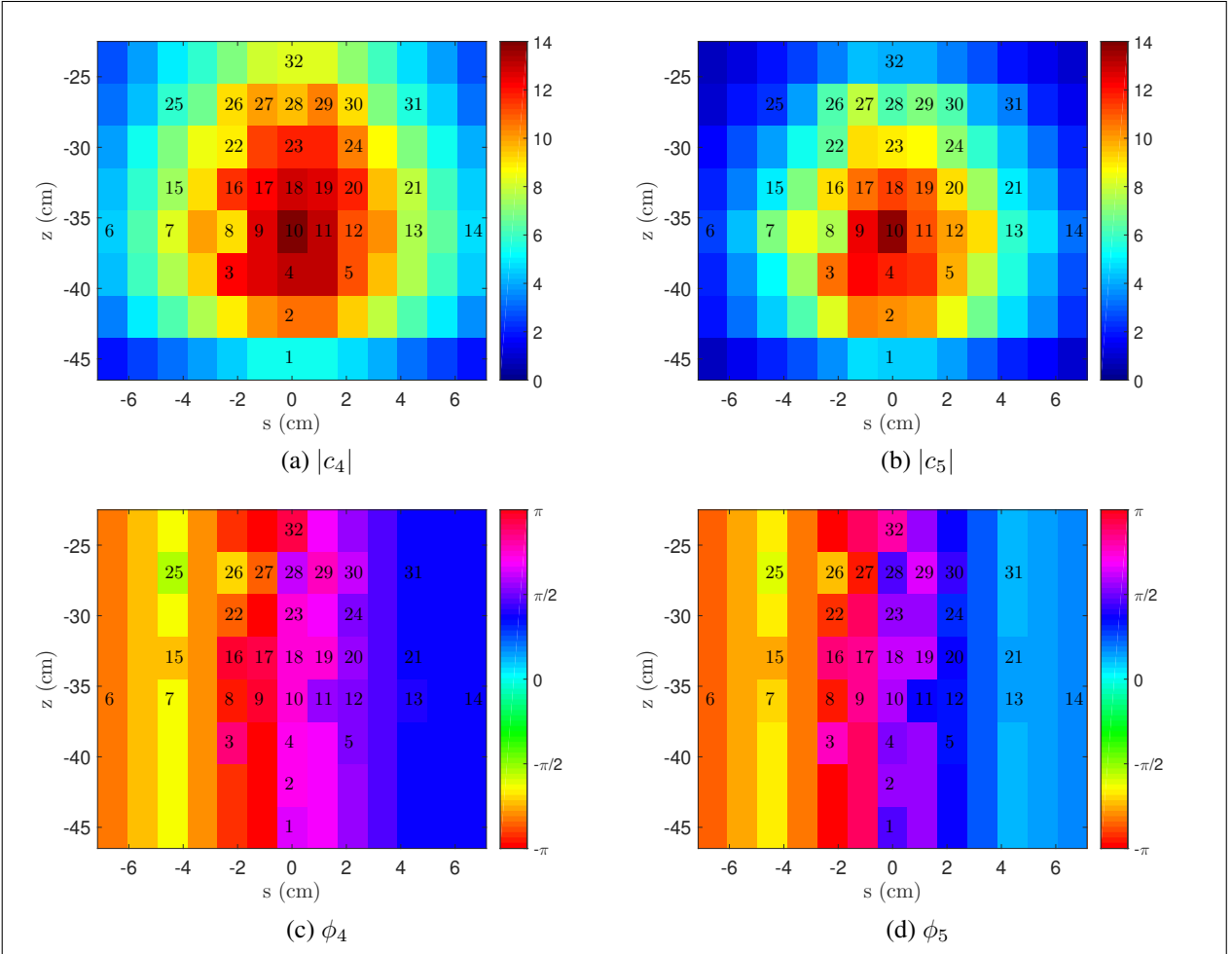


Figure 6. Map of the Fourier series coefficients $c_n = |c_n|e^{i\phi_n}$ of the harmonics 4 and 5 for $d = 2D/7$. The coefficients are either directly obtained from the 32 pressure tap measurements (as numbered) or obtained by an extrapolation procedure.

is only one pressure tap at the extreme values, this change of slope must be taken with care.

The distributions of the magnitude and phase of c_n with respect to s , as given in Figure 7 for harmonics 3 to 6, are used to obtain a complete map of the wall pressure containing $13 \times 8 = 104$ values, as shown in Figure 6 for the harmonics 4 and 5. Repeating the same procedure, similar maps are obtained for a blade-tower distance $d = D/2$ (not shown here). A similar pattern is observed at this greater distance, but the maximum value of $|c_n|$ is now close to 7 Pa instead of 14 Pa. It is however not possible to obtain such a map for $d = D$, as the signal to noise ratio is too low to obtain reliable results.

3.2 Acoustic pressure signals

The acoustic pressure signals recorded at microphones 1, 2 and 3 are also processed using TSA in order to improve the signal-to-noise ratio. The signals contain approximately 1300 periods of duration T_{BPF} , and TSA is performed on 100 successive periods, thus 13 averaged signals are obtained, from which the mean acoustic pressure can be deduced. The complex Fourier series coefficients are calculated from the mean acoustic pressure at each microphone.

The magnitude $|c_n|$ of the mean Fourier series coefficients are plotted in Figure 8 for various blade-tower distances d and compared to the reference case without tower. The tower is seen to have no effect on the fundamental frequency. The magnitude $|c_1|$ can indeed be attributed to steady loading noise, as shown in Ref. [5], with high values at microphone 1 and 3 that are close to the rotor plane. The blade-tower interaction noise is significant for $d \leq D/2$, with peak values for harmonics between 3 and 5. The blade-tower interaction noise is also noticeable at $d = D$ for microphones 1 and 3, but with much smaller values of $|c_n|$.

4. SEMI-ANALYTICAL MODEL FOR BLADE-TOWER INTERACTION NOISE

In order to predict the tonal noise from open rotors, the Ffowcs-Williams and Hawkings equation is often used. At low speeds, the loading noise term is generally dominant. Blade-tower interaction noise is an unsteady loading mechanism, as the presence of the tower causes a sudden change in the angle of attack seen by the blades. Furthermore, not only the rotating blades are radiating noise, but also the tower. Yauwenas et al. [2] and Zajamsek et al. [3] have

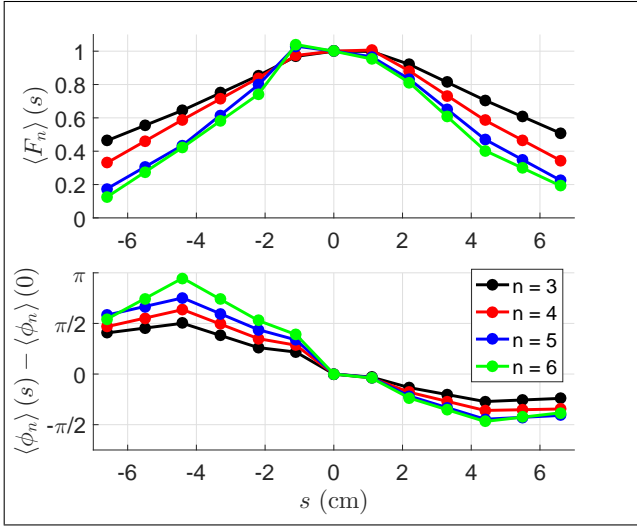


Figure 7. Evolution of the relative magnitude $\langle F_n \rangle(s)$, and of the phase $\langle \phi_n \rangle(s) - \langle \phi_n \rangle(0)$ with respect to s deduced from the mean over measurements at different heights.

even show that at blade-tower distances smaller than the tower diameter, the tower is the dominant source of blade-tower interaction noise.

In this study, we focus on the contribution of the tower, that is modeled using Curle's analogy in the geometric far-field approximation assuming the tower is acoustically compact. Even though the far-field approximation is not strictly valid for the lowest harmonics, it has been checked that the difference with the exact model is not significant. In the time domain, the acoustic pressure at microphone position $\mathbf{x} = (x_1, x_2, x_3)$ is given by [6, Eq. (4.4.7)]:

$$p(\mathbf{x}, t) \approx \frac{x_1}{4\pi|\mathbf{x}|^2 c_0} \left[\frac{\partial F_1}{\partial \tau} \right]_{\tau=\tau^*} + \frac{x_2}{4\pi|\mathbf{x}|^2 c_0} \left[\frac{\partial F_2}{\partial \tau} \right]_{\tau=\tau^*}, \quad (1)$$

$$F_1(\tau) = \int_0^{2\pi} \int_{-H}^0 p_w(\tau, \theta, z) \cos \theta \frac{D}{2} d\theta dz, \quad (2)$$

$$F_2(\tau) = \int_0^{2\pi} \int_{-H}^0 p_w(\tau, \theta, z) \sin \theta \frac{D}{2} d\theta dz, \quad (3)$$

where F_1 and F_2 are the forces applied by the tower surface to the fluid along the rotor axis (x) and perpendicular to the rotor axis (y), $\tau^* = t - |\mathbf{x}|/c_0$ is the emission time, with c_0 the sound speed, and $p_w(\tau, \theta, z)$ is the fluctuating wall pressure.

In the frequency domain, the acoustic pressure is first decomposed into Fourier series:

$$p(\mathbf{x}, t) = \sum_{k=-\infty}^{\infty} c_k(\mathbf{x}) e^{-ik\Omega t}, \quad (4)$$

where $\Omega = 2\pi/T_{BPF}$, and $c_n(\mathbf{x})$ are the complex Fourier coefficients given by:

$$c_n(\mathbf{x}) = \frac{\Omega}{2\pi} \int_0^{T_{BPF}} p(\mathbf{x}, t) e^{in\Omega t} dt. \quad (5)$$

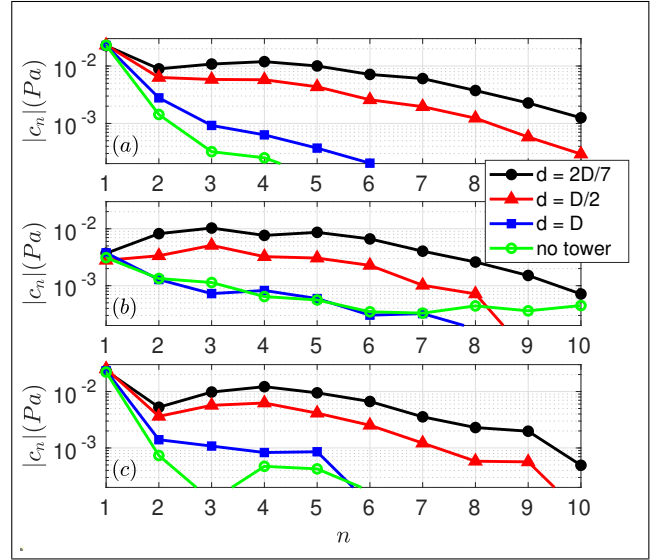


Figure 8. Magnitude of the Fourier series coefficients $|c_n|$ at microphones (a) 1, (b) 2 and (c) 3 for various blade-tower distances d .

After introducing Equation (1) into Equation (5), one obtains:

$$c_n(\mathbf{x}) \approx \frac{-in\Omega x_i f_{i,n}}{4\pi|\mathbf{x}|^2 c_0} e^{in\Omega|\mathbf{x}|/c_0}, \quad (6)$$

where $f_{i,n}$ are the Fourier series coefficients of the force $F_i(\tau)$.

5. RESULTS

First, the forces along x and y and the associated Fourier series coefficients are plotted in Figure 9 for $d = 2D/7$ and $d = D/2$. At both blade-tower distances, the two components of the force have similar values, with slightly higher Fourier coefficients for $F_1 = F_x$ below $n = 5$ and slightly higher Fourier coefficients for $F_2 = F_y$ above $n = 6$. The fact that the lateral force F_y has the same order of magnitude as the axial force F_x can be explained by the phase distribution of the wall pressure along the tower surface, as seen in Figure 6. From Equation (6), we can thus expect that the acoustic pressure in the rotor plane will be significant, as will be seen in the microphone 1 results.

The comparison between model and measurements at microphone 1 is shown in Figure 10. The magnitude of the Fourier series coefficients are first compared in Figure 10 for $d = 2D/7$ and $d = D/2$. As microphone 1 is in the rotor plane ($x_1 = x = 0$), only the force $F_2 = F_y$ contributes in Equation (6). At both blade-tower distances, the model predictions follow quite well the measurements, except for the fundamental component $n = 1$ as steady loading is not accounted for in the model. The model also tends to overpredict the amplitudes of the harmonics 4 and 5. The amplitudes of the harmonics 3 to 6 are 2 to 3 times larger at $d = 2D/7$ compared to $d = D/2$, in the predictions as in the measurements.

Then, the acoustic pressure waveforms are plotted in Figures 10(b) for $d = 2D/7$ and in Figures 10(c) for

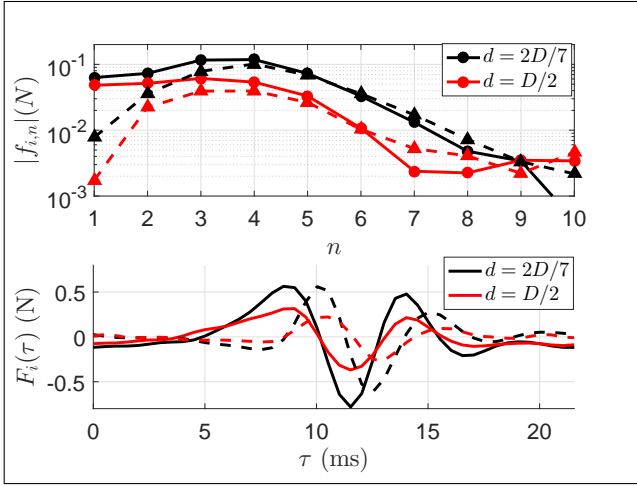


Figure 9. (a) Magnitude of the Fourier series coefficients $|f_{i,n}|$ and (b) corresponding forces $F_i(\tau)$ along x (solid lines) and y (dashed lines) for various blade-tower distances d .

$d = D/2$. In order to remove the influence of steady loading noise from the measurements, a Fourier synthesis is performed using only components 2 to 10 in the Fourier series. This enables to improve significantly the agreement between the model predictions plotted with blue dashed lines and the filtered measurements plotted with gray solid lines.

Figure 11 shows the comparison between model and measurements at microphone 2, that is on the rotor axis ($x_2 = y = 0$). As a result, only the force $F_1 = F_x$ contributes in Equation (6). At both blade-tower distances, the magnitude of the Fourier series coefficients are strongly overpredicted for harmonics 3 to 6, which explains that the predicted pressure waveforms have higher amplitudes than the measured ones. As steady loading does not contribute at this position, the filtered measurement is almost identical to the original measurement.

Finally, Figure 12 shows the comparison between model and measurements at microphone 3. As for microphone 2, only the force $F_1 = F_x$ contributes in Equation (6). At both blade-tower distances, the magnitude of the Fourier series coefficients predicted by the model agree quite well with the measurements, except at $n = 1$ due to the steady loading noise, and at $n = 4$ and 5 where the magnitude is overpredicted. The predicted waveforms agree relatively well with the filtered measurements.

The discrepancies between model predictions and measurements can be due to various reasons. First, the extrapolation procedure used to obtain the wall pressure maps is prone to errors, as there is a limited number of measurements at large values of s . Second, only the contribution of the tower is included in the blade-tower interaction noise model. In a similar configuration but with a pitch angle of 0° , Yauwenas *et al.* [2] show in their Figure 14 that the contribution from the blades, although small compared to the contribution from the tower, is not negligible. Furthermore, both contributions are out of phase. As a result, this

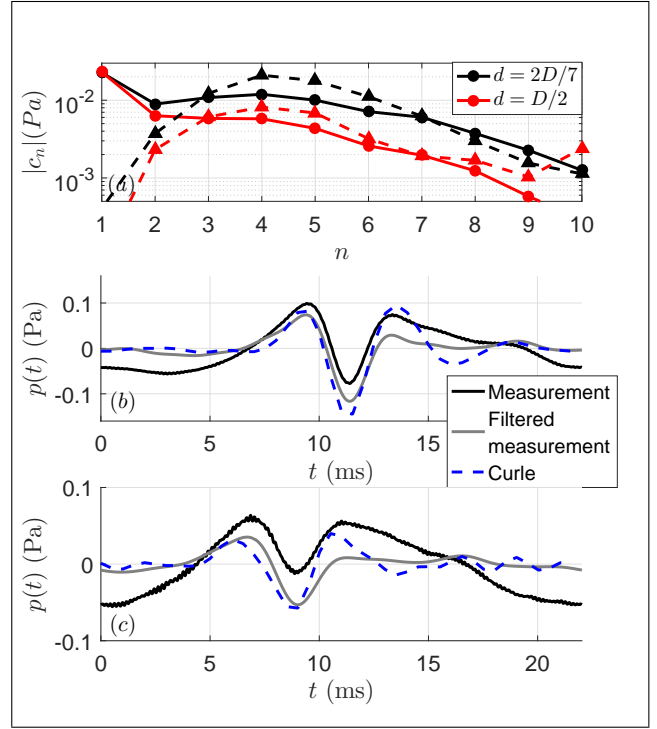


Figure 10. (a) Magnitude of the Fourier series coefficients $|c_n|$ for the measurements (solid lines) and for the model predictions (dashed lines), and acoustic pressure waveforms at (b) $d = 2D/7$ and (c) $d = D/2$ for microphone 1.

is a plausible explanation for the overprediction that is observed in our case study.

6. CONCLUSION AND PERSPECTIVES

In this paper, blade-tower interaction noise has been characterized experimentally in an open rotor test bench installed in the anechoic chamber of ENSTA Paris. The blade pitch is set to 3° , which means that the induced flow is small and that the blade passage effect is dominating the effect of the reduced velocity in the vicinity of the tower. The blade-tower distance d has been varied between $2D/7$ and D , where D is the tower diameter, to study its influence on the radiated noise. The acoustic pressure has been measured using three microphones, and the wall pressure on the tower has been obtained using 32 pressure taps distributed on its surface.

The wall pressure on the tower surface has been processed using time-synchronous averaging in order to improve the signal to noise ratio. Clean signals have been obtained at $d = 2D/7$ and $d = D/2$, but not at $d = D$ because the signals are buried in the noise. Fourier series decomposition show that the maximum amplitudes are obtained at the harmonics 4 or 5 with respect to the blade passing frequency. Based on the mean distribution of the magnitude $|c_n|$ and the phase ϕ_n along the curvilinear abscissa s , an extrapolation procedure is proposed to obtain a complete map of the wall pressure on the tower surface. The wall pressure on the tower surface is found to be maximum at 80% of the blade span. The acoustic pressure sig-

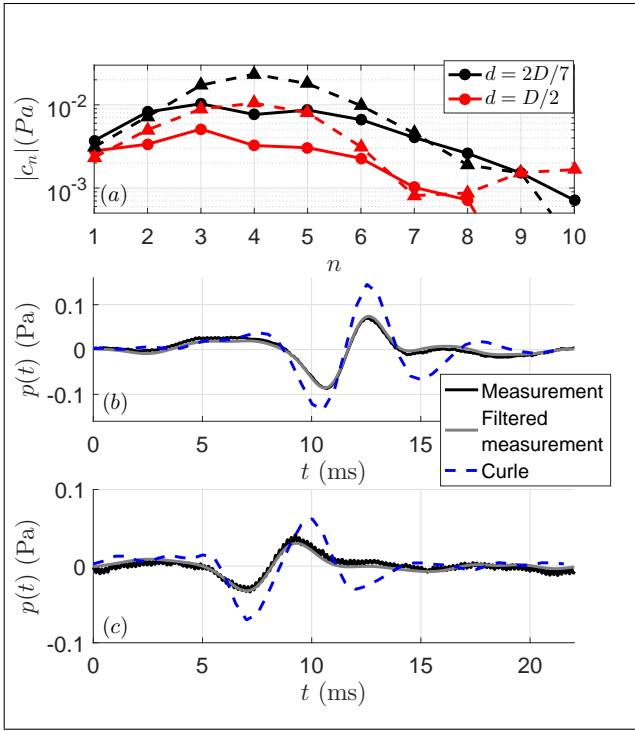


Figure 11. (a) Magnitude of the Fourier series coefficients $|c_n|$ for the measurements (solid lines) and for the model predictions (dashed lines), and acoustic pressure waveforms at (b) $d = 2D/7$ and (c) $d = D/2$ for microphone 2.

nals are processed in a similar fashion. The blade-tower interaction noise is significant when $d \leq D/2$ for all three microphones.

Using the frequency-domain Curle’s analogy in the geometric far-field approximation and assuming the tower is acoustically compact, the acoustic pressure is calculated based on the Fourier series coefficients of the wall pressure. The contribution of the blades in the noise generation is not considered. The measured and predicted spectra are in good agreement, although the magnitude of the Fourier series coefficients of harmonics 3 to 6 tends to be overpredicted. In order to remove steady loading noise from the measurements, a Fourier synthesis of the acoustic pressure is performed on harmonics 2 to 10 only. The acoustic pressure waveforms predicted by the model follow relatively well the filtered measurements, although the amplitudes are too large, especially for the microphone on the rotor axis.

In the future, the contribution of the blades in the noise generation will be added in order to improve the agreement between model predictions and measurements. This can be done analytically using simplified unsteady aerodynamic theories [7], or numerically using for instance the sliding mesh method [2, 3].

7. REFERENCES

[1] H. Madsen, “Low Frequency Noise from Wind Turbines Mechanisms of Generation and its Modelling,”

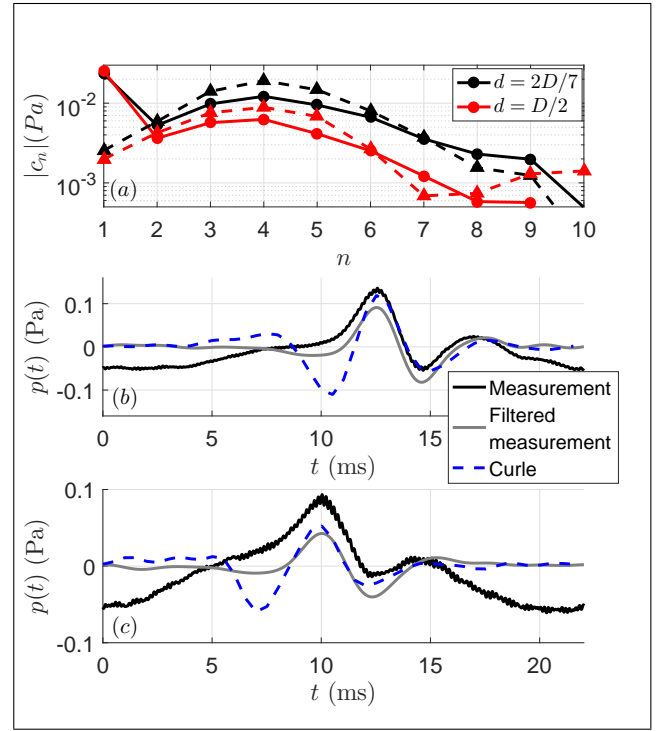


Figure 12. (a) Magnitude of the Fourier series coefficients $|c_n|$ for the measurements (solid lines) and for the model predictions (dashed lines), and acoustic pressure waveforms at (b) $d = 2D/7$ and (c) $d = D/2$ for microphone 3.

Journal of Low Frequency Noise Vibration and Active Control, vol. 29, no. 4, pp. 239–251, 2010.

- [2] Y. Yauwenas, B. Zajamšek, J. Reizes, V. Timchenko, and C. J. Doolan, “Numerical simulation of blade-passage noise,” *The Journal of the Acoustical Society of America*, vol. 142, no. 3, pp. 1575–1586, 2017.
- [3] B. Zajamsek, Y. Yauwenas, C. J. Doolan, K. L. Hansen, V. Timchenko, J. Reizes, and C. H. Hansen, “Experimental and numerical investigation of blade–tower interaction noise,” *Journal of Sound and Vibration*, vol. 443, pp. 362–375, 2019.
- [4] M. Roger and S. Moreau, “Tonal-noise assessment of quadrotor-type uav using source-mode expansions,” *Acoustics*, vol. 2, pp. 674–690, 2020.
- [5] C. Deora, “Experimental characterization and analytical modelling of rotor tonal noise,” 2019. MSc Thesis Report, TU Delft.
- [6] S. Glegg and W. Devenport, *Aeroacoustics of Low Mach Number Flows*. Academic Press, 2017.
- [7] M. Roger and K. Kucukcoskun, “Near-and-far field modeling of advanced tail-rotor noise using source-mode expansions,” *Journal of Sound and Vibration*, vol. 453, pp. 328–354, 2019.